Supplement of Atmos. Chem. Phys., 23, 7551–7568, 2023
https://doi.org/10.5194/acp-23-7551-2023-supplement

Atmospheric Chemistry and Physics
Open Access
EGU

Supplement of

Evolution and chemical characteristics of organic aerosols during wintertime $PM_{2.5}$ episodes in Shanghai, China: insights gained from online measurements of organic molecular markers

Shuhui Zhu et al.

Correspondence to: Jian Zhen Yu (jian.yu@ust.hk) and Cheng Huang (huangc@saes.sh.cn)

Text S1. Measurement principles and operational procedures of online instruments employed in the study

The operational procedure of the TAG system has been provided in section 2.1 in the main paper. In this study, a total of 98 organic molecules in $PM_{2.5}$ were quantified by the TAG system. Calibration curves were first established before using the TAG system to measure ambient samples. To be specific, 5 μL of ISs was mixed with 0-5 loops (5 uL/loop) of external standards and co-injected into CTD cell for GC-MS identification and quantification. This yielded a five-point calibration curve for each analyte. Calibration curves were established by fitting the normalized peak areas of external standards to their corresponding IS with respective concentrations. During the ambient measurements, 1 loop (5 μL) of IS was also injected into each aerosol sample by the auto-injection system equipped in the TAG. The target organic compounds in aerosol samples were identified by their retention times and mass spectra, which were obtained using authentic standards. Then we calculated peak area ratios of target organic compounds against their corresponding IS (listed in Table S1) for each ambient sample and used the above-mentioned calibration curves to quantify their masses in real aerosol samples. The details of the TAG calibration and quantification method have been given in several of our previously published papers (He et al., 2020; Wang et al., 2020).

An Aerosol Mass Spectrometer (AMS) was deployed to quantify major components in PM_1 during the campaign. The AMS was operated alternately between V & pToF combined mode and W mode for 150 s each. Filtered ambient air was sampled and analyzed before and after the campaign for 30 min with a HEPA-filter placed in front of the inlet, defined as the filter periods. The gas-phase CO_2 contribution to the CO_2^+ signal was corrected by the data during the filter periods and the detection limits of species are defined as three times the standard deviation of the measured species concentrations in the filter periods, which were 0.19, 0.033, 0.067, 0.182, and 0.032 $\mu g/m^3$ for organic, sulfate, nitrate, ammonium, and chloride, respectively. The PMF2 algorithm with a toolkit (version 3.04A) based on Igor Pro software was applied to perform PMF analysis of AMS mass spectra. More detail descriptions of AMS-PMF analysis during this measurement period have been reported by Huang et al (2021) and the PMF analysis results are given in Figure S1.

For volatile organic compounds, two on-line gas chromatograph with flame ionization detector (GC-FID) systems (Chromato-sud airmoVOC C2-C6 #5250308 and airmoVOC C6-C12 #2260308, Chromatotec, Bordeaux, France) were employed to provide their mass concentrations continuously with 30 min time resolution. The C_2 - C_6 VOCs were collected through a preconcentration trap containing porous substances (Carbotrap C, Carbopack B and Carboxen). The trap was cooled by a cell with Peltier effect during the sampling period. After sampling, it was heated to 220 ℃ to thermally desorb trapped C_2 - C_6 VOCs. For the C_6 - C_{12} VOCs, they were collected with a trap filled with Carbotrap B, which was also cooled during the sampling period while heated to 380 ℃ during the thermal desorption step. The desorbed C_2 - C_6 and C_6 – C_{12} VOC compounds were then separated on ultimetal column and quantified by flame ionization detector (FID). Calibrations were conducted automatically once a day with three internal permeation tubes containing standard compounds during the campaign. Additionally, manual calibrations by standard gas (Spectra, USA) were also performed before and after the campaign.

Major components and trace elements in $PM_{2.5}$ were measured in this study with hourly time-resolution. Among them, water-soluble inorganic ions, including Cl^-, NO_3^-, SO_4^{2-}, Na^+, NH_4^+, K^+, Mg^{2+}, and Ca^{2+}, were measured by a commercial instrument for online monitoring of aerosols and gases (MARGA, model ADI 2080, Applikon Analytical B.V.). In this instrument, aerosol samples were first drawn through a wet rotating annular

denuder (WRD) where water-soluble gases diffused to the absorption solution (0.0035% H_2O_2), then particles were collected in a stream-jet aerosol collector (SJAC). After sampling, the absorption solutions were drawn from the WRD and the SJAC to syringes and subsequently injected to ion chromatographs with an internal standard (LiBr) for quantifications.

OC and EC in $PM_{2.5}$ were monitored using a semicontinuous OC/EC analyzer (model RT-4, Sunset Laboratory Inc.) equipped with a $PM_{2.5}$ cyclone and an upstream parallel-plate organic denuder (Sunset Laboratory Inc.). Ambient $PM_{2.5}$ was sampled on a quartz filter in the oven at a flow rate of 8.0 L/min. Then the sample was analyzed by the thermal-optical transmittance method (TOT) using a two-stage thermal procedure that consisted of 600 - 840 °C in a helium atmosphere and 550 - 650 - 870 °C in an oxidizing atmosphere (2% oxygen in helium).

A total of 15 trace elements (K, Ca, V, Cr, Mn, Fe, Ni, Cu, Zn, As, Se, Ba, Pb, Si, and S) in $PM_{2.5}$ were measured at the site using an online non-destructive X-ray fluorescence spectrometer (XRF, model Xact 625, Cooper Environmental), which employs a reel-to-reel method to sample and analyze elements. $PM_{2.5}$ samples were pumped through a section of Teflon filter tape at a flow rate of 16.7 L/min. Then the section of filter tape was analyzed by non-destructive X-Ray Fluorescence. The sampling and analysis processes occurred simultaneously, producing hourly data for the monitored trace elements.

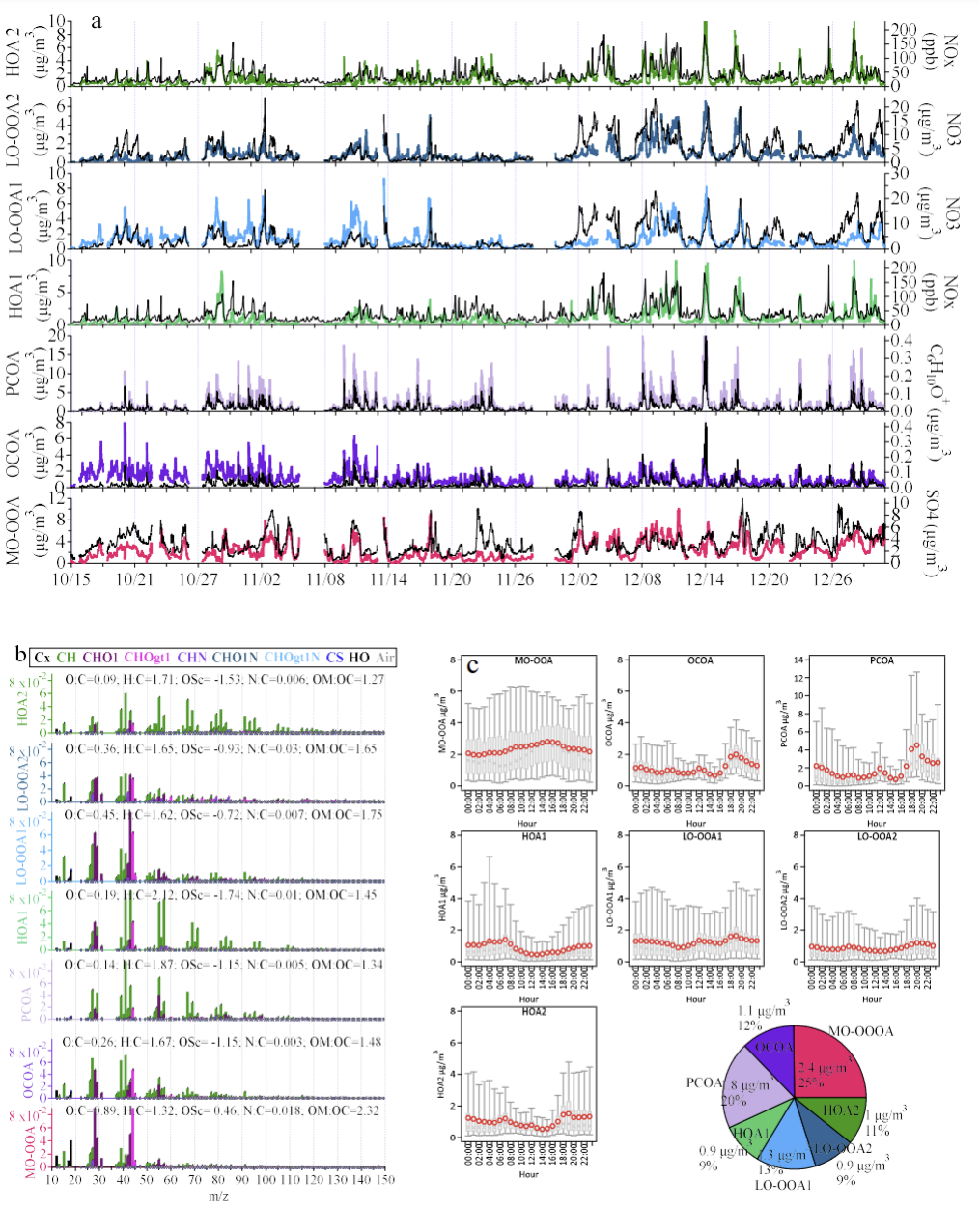

Figure S1. (a) Time series, (b) mass spectral profiles, (c) diurnal variations and fractional contributions of the OA factors from the 7-factor solution of AMS-PMF analysis. Adapted from Huang et al. (2021) figure S2.

Table S1. Statistics of hourly concentrations of 98 organic molecules measured by TAG system.

Group	Compounds	Abbreviation	Avg ng/m^3	Range ng/m^3	Internal standards	Quantification ions	Potential sources
L_DCAs	Malonic acid	C3	0.66	0.04-5.54	Adipic acid-d10	233	Oxidation products of VOCs
	Succinic acid	C4	77.8	3.50-498.4	Succinic acid-d4	247	
	Glutaric acid	C5	16.1	0.73-150.6		261	
L_hDCAs	Malic_acid	hC4	155.5	10.1-568.1	Azelaic Acid-d14	233	Oxidation products of VOCs
	Citramalic_acid	hiC5	29.4	2.16-142.1		247	
	Glyceric_acid	hC3	53.5	3.33-234.5	Succinic acid-d4	292	
	2-hydroxyglutaric acid	2-hC5	2.26	0.04-13.7	Adipic acid-d10	349	
	3-hydroxyglutaric acid	3-hC5	23.7	0.70-170.6		349	
H_DCAs	Adipic acid	C6	9.54	0.71-64.4	Adipic acid-d10	111	Oxidation products of VOCs
	Pimelic acid	C7	2.22	0.17-15.5	Azelaic Acid-d14	289	
	Suberic acid	C8	4.05	0.08-26.6		303	
H_hDCAs	2-hydroxyadipic acid	2-hC6	3.06	0.05-22.9	Adipic acid-d10	363	Oxidation products of VOCs
	3-Hydroxyadipic acid	3-hC6	15.4	0.40-116.4		363	
	Hydroxypimelic acid	hC7	6.95	0.30-39.4	Azelaic Acid-d14	377	
αPinT	Pinic acid	PA	7.55	0.38-34.3	Azelaic Acid-d14	171	Oxidation products of α-pinene
	Pinonic acid	PNA	1.03	0.09-6.47		171	
	3-methyl-1,2,3-butanetricarboxylic acid	3-MBTCA	4.34	0.10-26.0		405	
	3-acetylglutaric acid	3-AGA	3.73	0.40-15.1		303	
	3-hydroxy-4,4-dimethylglutaric	3-HDGA	12.6	0.06-67.3		377	
βCaryT	β-caryophyllinic acid	b-CA	1.36	BD-5.15	Azelaic Acid-d14	383	Oxidation product of β-caryophyllene
DHOPA	2,3-dihydroxy-4-oxopentanoic acid	DHOPA	12.9	0.47-58.6	Azelaic Acid-d14	277	Oxidation product of mono-aromatics
Pht	Phthalic acid	Pht	28.8	1.28-147.1	Phthalic-3,4,5,6-d4	295	Oxidation product of

					acid		naphthalene and derivatives
Aromatic polycarboxylic acids (Ar-PCAs)	Isophthalic acid	iPh	1.75	0.12-9.14	Phthalic-3,4,5,6-d4 acid	295	Oxidation products of aromatic compounds
	Terephthalic acid	tPh	21.1	0.94-105.3		295	
	1,2,4-benzentricarboxylic acid	124BTCA	15.1	0.25-98.4		411	
	1,3,5-benzentricarboxylic acid	135BTCA	2.49	0.16-15.1		411	
Nitro-aromatic compounds (NACs)	4-nitrocatechol	4NC	1.54	BD-9.42	Phthalic-3,4,5,6-d4 acid	284	Nitration of aromatic compounds
	4-nitrophenol	4NP	3.33	0.06-20.7		196	
	3-methyl-5-nitrocatechol	3M5NC	0.24	BD-1.30		298	
	4-methyl-5-nitrocatechol	4M5NC	0.66	BD-4.00		298	
Biomass burning tracers (BBtracers)	3-hydroxybenzoic acid	3-HBA	0.76	0.05-3.36	Phthalic-3,4,5,6-d4 acid	267	Biomass burning
	4-hydroxybenzoic acid	4-HBA	1.40	0.09-6.41		267	
	Syringic acid	SyrinA	0.65	0.02-3.97		327	
	Vanillic acid	VaniA	0.57	0.03-3.27		267	
	Galactosan	Gal	2.44	0.13-12.8	Levoglucosan-d7	217	
	Mannosan	Manno	4.54	0.36-19.4		204	
	Levoglucosan	Levo	61.3	5.18-185.1		204	
Primary sugars	Mannitol	Manni	31.3	1.92-155.0	Glucose-d7	319	Plant debris, fungal spores
	Glucose	Glu	5.17	0.51-21.8		204	
C_9 acids	Azeleic_acid	C9	10.5	1.02-62.1	Azelaic Acid-d14	317	Oxidation products of long-chain fatty acids
	9-oxononanoic acid	ωC9:0	5.95	0.45-36.4		228	
	Nonanoic acid	C9:0	0.58	0.04-5.05		215	
Saturated fatty acids (sFAs)	Decanoic acid	C10:0	2.00	0.14-12.6	Azelaic Acid-d14	229	Cooking
	Undecanoic acid	C11:0	0.06	BD-0.32		243	
	Lauric acid	C12:0	0.86	0.05-6.26	Myristic acid-d27	257	
	Tridecanoic acid	C13:0	0.11	0.02-0.58		271	
	Myristic acid	C14:0	2.92	0.18-21.6		285	
	Pentadecanoic acid	C15:0	0.85	0.10-5.88	Palmitic acid-d31	299	
	Palmitic acid	C16:0	53.9	4.39-360.8		313	

	Heptadecanoic acid	C17:0	0.93	0.05-9.98		327	
	Stearic acid	C18:0	30.2	2.20-283.0		341	
	Nonadecanoic acid	C19:0	0.34	0.03-3.68	Stearic acid-d35	355	
	Eicosanoic acid	C20:0	0.84	0.04-10.1		369	
Unsaturated fatty acids (uFAs)	Oleic acid	C18:1	20.5	0.64-178.2	Stearic acid-d35	339	Cooking
	Palmitoleic acid	C16:1	0.36	0.03-3.31	Palmitic acid-d31	311	
	Linoleic acid	C18:2	7.76	0.07-164.6	Stearic acid-d35	337	
Alkanes	Heneicosane	n-C21	0.99	0.20-5.35	n-Eicosane-d42	57	Vegetative detritus, fossil fuel uses
	Docosane	n-C22	1.94	0.29-9.29		57	
	Tricosane	n-C23	1.95	0.25-11.6		57	
	Tetracosane	n-C24	3.05	0.43-13.5	n-Tetracosane-d50	57	
	Pentacosane	n-C25	4.73	0.67-25.6		57	
	Hexacosane	n-C26	4.12	0.48-22.0		57	
	Heptacosane	n-C27	4.65	0.52-25.8		57	
	Octacosane	n-C28	3.41	0.26-22.3		57	
	Nonacosane	n-C29	4.36	0.29-23.9		57	
	Tracotane	n-C30	2.38	0.02-17.2	n-Octacosane-d58	57	
	Hentriacontane	n-C31	2.01	0.02-12.5		57	
	Dotriacontane	n-C32	1.39	0.02-13.4		57	
	Tritractotane	n-C33	0.73	BD-5.67		57	
	Tetratriactoane	n-C34	0.60	0.02-4.37		57	
	Pentatriacontane	n-C35	0.56	BD-4.39	n-Hexatriacontane-d74	57	
	Hexatriacontane	n-C36	0.38	BD-2.91		57	
	Heptatriacontane	n-C37	0.22	BD-2.36		57	
Hopanes	22,29,30-trisnorhopane	C27Tm	0.04	BD-0.26	n-Tetracosane-d50	191	Vehicular emission, coal combustion
	αβ-norhopane	C29αβ	0.37	0.03-1.96		191	
	αβ-hopane	C30αβ	0.46	BD-2.32		191	
	αβ-22S-homohopane	C31αβS	0.11	BD-0.66		191	

	αβ-22R-homohopane	C31αβR	0.11	BD-0.70		191	
PAHs	Phenanthrene	Phe	0.43	0.07-1.34	Phenanthrene-d10	178	Combustion sources (e.g., coal combustion)
	Anthracene	Ant	0.18	0.01-0.54		178	
	Fluoranthene	Flu	0.41	0.03-3.38		202	
	Pyrene	Pyr	0.38	BD-3.48		202	
	Benzo[b]chrysene	BbC	0.02	BD-0.31		278	
	Benzo[c]phenanthrene	BcP	0.05	BD-0.40		228	
	Cyclopenta[cd]pyrene	CcdP	0.07	BD-0.86		226	
	Dibena[a,c]anthracene	DacA	0.02	BD-0.42		278	
	Triphenylene	TriP	0.18	BD-2.39		228	
	Chrysene	Chr	0.22	0.02-1.26	Chrysene-d12	228	
	Benzo[a]anthracene	BaA	0.17	BD-1.46		228	
	Benzo[b]fluoranthene	BbF	0.23	0.01-1.48		252	
	Benzo[k]fluoranthene	BkF	0.43	BD-2.69		252	
	Benzo[a]fluoranthene	BaF	0.12	BD-1.14	Perylene-d12	252	
	Benzo[e]pyrene	BeP	0.42	0.03-2.49		252	
	Benzo[a]pyrene	BaP	0.45	BD-3.85		252	
	Perylene	Per	0.18	BD-1.81		252	
	Indeno[1,2,3-cd]pyrene	IcdP	0.38	BD-3.15	Benzo[ghi]perylene -d12	276	
	Benzo[ghi]perylene	BghiP	0.53	0.04-2.47		276	
	Dibenzo[a,h]anthracene	DahA	0.09	BD-1.08		278	

Table S2. Statistics of hourly concentrations of all VOC species measured by GC-FID and their corresponding subgroups.

Subgroups	Species	Avg ppb	Range ppb
Alkanes	Ethane	6.91	0.22-33.6
	Propane	5.47	0.16-51.6
	Isobutane	1.39	0.06-10.2
	n-Butane	1.82	0.09-18.8
	Cyclopentane	0.10	BD-1.20
	Isopentane	0.87	0.06-6.19
	n-Pentane	0.60	0.01-3.15
	2,2-Dimethylbutane	0.04	BD-0.97
	2,3-Dimethylbutane	0.07	BD-0.97
	2-Methylpentane	0.18	BD-1.18
	3-Methylpentane	0.18	BD-1.00
	n-Hexane	0.30	0.02-2.00
	2,4-Dimethylpentane	0.03	BD-1.04
	Methylcyclopentane	0.09	BD-0.98
	2-Methylhexane	0.08	BD-1.01
	Cyclohexane	0.15	BD-1.51
	2,3-Dimethylpentane	0.03	BD-1.01
	3-Methylhexane	0.08	BD-1.79
	2,2,4-Trimethylpentane	0.05	BD-1.01
	n-Heptane	0.13	BD-3.09
	Methylcyclohexane	0.09	BD-1.01
	2,3,4-Trimethylpentane	0.04	BD-1.03
	2-Methylheptane	0.03	BD-1.05
	3-Methylheptane	0.03	BD-1.06
	n-Octane	0.10	0.01-3.46
	n-Nonane	0.18	0.01-3.88
	n-Decane	0.08	0.01-1.08
Alkenes	Ethylene	2.49	0.04-27.0
	Propylene	0.63	BD-11.9
	Trans-2-butene	0.08	BD-1.38
	1-Butene	0.12	BD-1.10
	Isobutylene	0.14	0.02-0.53
	cis-2-Butene	0.06	BD-1.10
	1,3-Butadiene	0.03	BD-0.40
	1-Pentene	0.03	BD-1.19
	trans-2-Pentene	0.03	BD-1.19
	Isoprene	0.04	BD-1.10
	cis-2-Pentene	0.02	BD-1.15
	1-Hexene	0.02	BD-0.96
	3-Methyl-1-butene	0.01	BD-0.06

	2-Methyl-1-butene	0.02	BD-0.11
	2-Methyl-2-butene	0.01	BD-0.23
	4-Methyl-1-pentene	0.002	BD-0.02
	2-Methyl-1-pentene	0.02	BD-0.47
	2-Methyl-2-pentene	0.001	BD-0.02
Acetylene	Acetylene	2.08	0.02-19.3
Aromatics	Benzene	0.59	0.04-1.94
	Toluene	1.21	0.06-7.35
	Ethylbenzene	0.38	0.02-5.39
	m/p-Xylene	0.70	BD-10.8
	o-Xylene	0.32	0.02-3.54
	Styrene	0.09	BD-0.95
	iso-Propylbenzene	0.03	BD-1.03
	n-Propylbenzene	0.05	BD-1.01
	m-Ethyltoluene	0.06	BD-1.10
	p-Ethyltoluene	0.05	BD-1.06
	1,3,5-Trimethylbenzene	0.05	BD-1.05
	o-Ethyltoluene	0.05	BD-1.01
	1,2,4-Trimethylbenzene	0.07	BD-0.91
	1,2,3-Trimethylbenzene	0.06	BD-1.00
	m-Diethylbenzene	0.04	BD-1.02
	p-Diethylbenzene	0.05	BD-0.92
OVOCs	Acetaldehyde	0.84	0.08-5.36
	Acrolein	0.10	BD-0.51
	Propanal	0.23	0.05-1.05
	n-Butanal	0.09	0.01-0.56
	Methacrolein	0.02	BD-0.14
	Methylvinylketone	0.03	BD-0.20
	Methylethylketone	0.80	0.02-6.87
	2-Pentanone	0.02	BD-0.13
	n-Pentanal	0.06	BD-0.36
	3-Pentanone	0.02	BD-0.07
	Methyl isobutyl ketone	0.04	BD-0.38
	n-Hexanal	0.16	0.01-1.85
	Methyl tert-butyl ether	0.15	BD-1.86
	Isopropyl alcohol	0.39	0.03-10.9
	Methyl acetate	0.53	0.01-16.2
	Ethyl acetate	0.95	0.01-15.1
	n-Propyl acetate	0.18	BD-7.44
	n-Butyl acetate	0.37	0.01-2.98
	Methyl methacrylate	0.01	BD-0.14
	Vinyl acetate	0.01	BD-0.28
	Acetonitrile	0.53	0.05-19.3
XVOCs	Freon-114	0.01	BD-0.04

Chloromethane	0.17	0.01-0.89
Vinylchloride	0.01	BD-0.13
Bromomethane	0.01	BD-0.16
Chloroethane	0.04	BD-2.06
Freon-11	0.62	0.01-22.1
1,1-Dichloroethene	0.003	BD-0.07
Freon-113	0.06	BD-0.21
Dichloromethane	1.58	0.05-14.6
1,1-Dichloroethane	0.01	BD-0.19
cis-1,2-Dichloroethene	0.003	BD-0.04
Chloroform	0.25	BD-26.1
1,1,1-Trichloroethane	0.002	BD-0.01
Carbontetrachloride	0.14	BD-7.65
1,2-Dichloroethane	0.54	0.01-5.97
Trichloroethylene	0.07	BD-2.46
1,2-Dichloropropane	0.14	BD-5.25
Bromodichloromethane	0.003	BD-0.01
trans-1,3-Dichloropropene	0.003	BD-0.14
cis-1,3-Dichloropropene	0.003	BD-0.06
1,1,2-Trichloroethane	0.03	BD-0.32
Tetrachloroethylene	0.11	0.01-8.88
1,2-Dibromoethane	0.002	BD-0.03
Chlorobenzene	0.03	BD-0.43
1,3-Dichlorobenzene	0.02	0.01-0.09
Benzylchloride	0.03	0.01-0.22
1,2-Dichlorobenzene	0.03	0.01-0.17

80

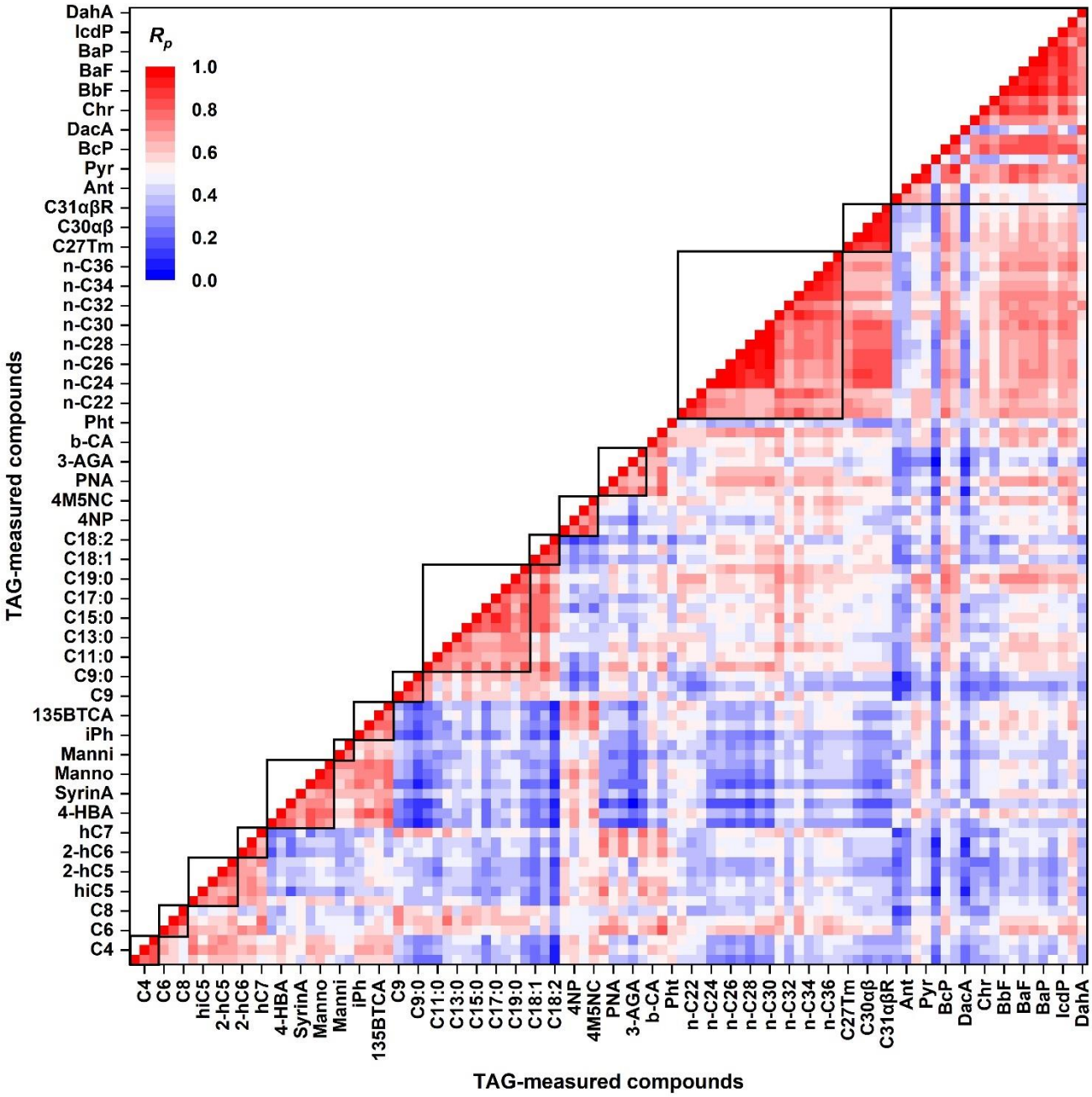

Figure S2. Pearson coefficients (R_p) of hourly concentrations 98 TAG-measured organic molecules. Organic molecules in each dark square box characterized by high Rp are classified into the same organic molecular group. The order of organic molecules is same with Table S2.

85

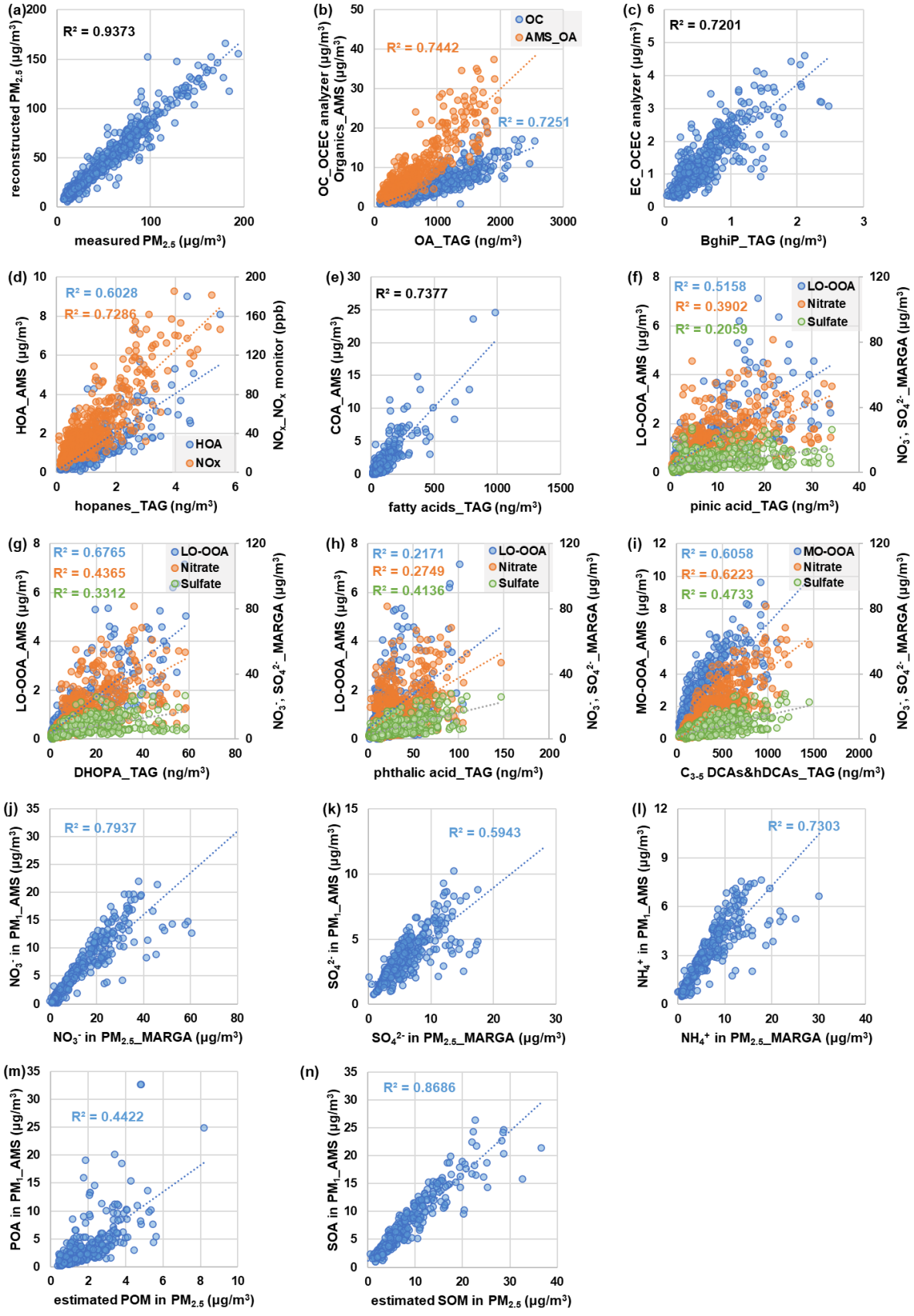

Figure S3. Scatter plots of select pairs of measured parameters with known underlying physical relationships. They serve as internal data consistency check.

Text S2. Clustering analysis and concentration weighted trajectory (CWT)

For every hour during the field campaign, a 48-hour backward trajectory starting at 100 m above the observation site was calculated by HYSPLIT software with 6-hour archived GDAS data as meteorological input. Then all the backward trajectories were clustered by calculating their spatial dissimilarity (SPVAR) and total spatial dissimilarity (TSV):

$$SPVAR = \sum_{j=1}^{x} \sum_{i=1}^{t} D_{ij}^2 \quad (1)$$

where D_{ij} is the distance from the stop point at the j^{th} hour in the i^{th} trajectory to the corresponding point in the average trajectory, t is the length of the trajectory, x is the number of trajectories in the cluster. Then TSV as shown in Figure S4 is calculated by summing up the SPVAR values of all clusters. The variations of $PM_{2.5}$ chemical composition under each cluster is given in Figure S5. Apparently, $PM_{2.5}$ chemical compositions were diverse under different air mass clusters with higher mass fractions of secondary organic matter (SOM) and sulfate observed under cluster 1 (CL#1). In comparison, cluster 2 (CL#2) was characterized by significantly higher mass loading of nitrate, and cluster 3 (CL#3) was characterized by higher mass percentages of elemental carbon (EC) and primary organic matter (POM). For cluster 4 (CL#4), higher mass proportions of sulfate and chloride were observed.

The potential source areas for $PM_{2.5}$ in Shanghai under the influence of different air mass clusters were then analyzed and illustrated by concentration weighted trajectory (CWT) approach with the adoption of ZeFir software based on the results derived from HYSPLIT. With the input of hourly $PM_{2.5}$ concentration data, the residence time of a back trajectory arriving at Shanghai in each 0.2° × 0.2° grid cell of a 25-50°N × 105-135°E geographical domain is determined via the following equation:

$$CWT_{ij} = \frac{\sum_{L=1}^{M} C_L \tau_{ij-L}}{\sum_{L=1}^{M} \tau_{ij-L}} \quad (2)$$

where CWT_{ij} is the attributed $PM_{2.5}$ concentrations in the ij^{th} grid cell, L is the index of the trajectory, M is the total number of back trajectories over a time period, C_L is the hourly concentration of $PM_{2.5}$ corresponding to the arrival of back trajectory L, $\tau_{ij\text{-}L}$ is the number of trajectory segment endpoints in the ij^{th} grid cell for back trajectory L.

A weighted function was applied to downweigh cells associated with low values of n_{ij} to lower uncertainties, which was based on the trajectory density by calculating log(n+1) as described by Bressi et al. (2014) and Waked et al. (2014). The weighted function is empirically determined using the following equations:

$$W = \begin{cases} 1, & for\ \log(n+1) > 0.85 * max_{\log(n+1)} \\ 0.725, & for\ 0.6 * max_{\log(n+1)} < \log(n+1)\ 0.85 * max_{\log(n+1)} \\ 0.475, & for\ 0.35 * max_{\log(n+1)} < \log(n+1)\ 0.6 * max_{\log(n+1)} \\ 0.175, & for\ \log(n+1) < 0.35 * max_{\log(n+1)} \end{cases} \quad (3)$$

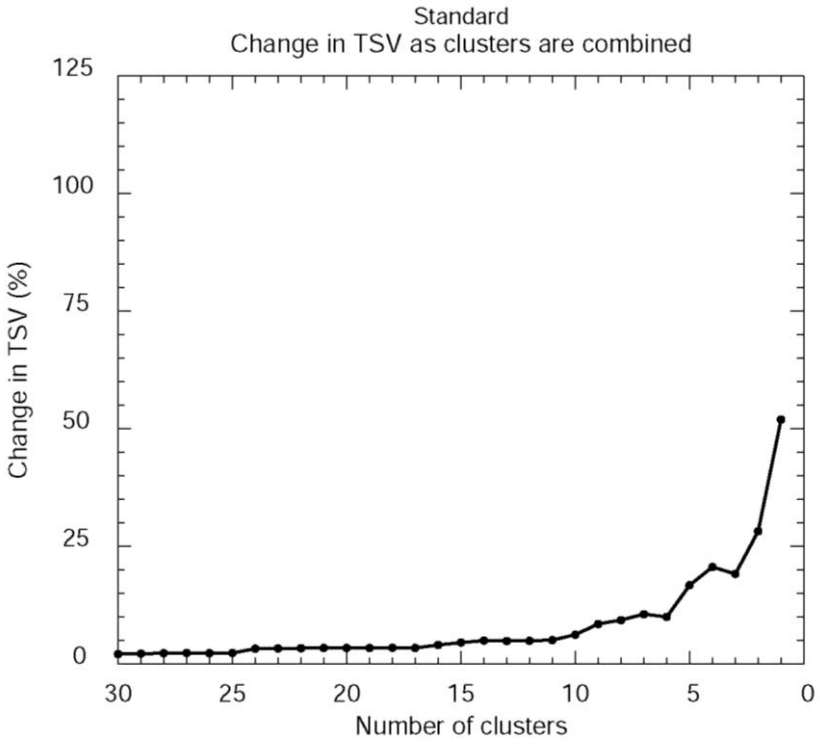

Figure S4. Change of total spatial variance (TSV) as a function of number of clusters for 100m arrival heights.

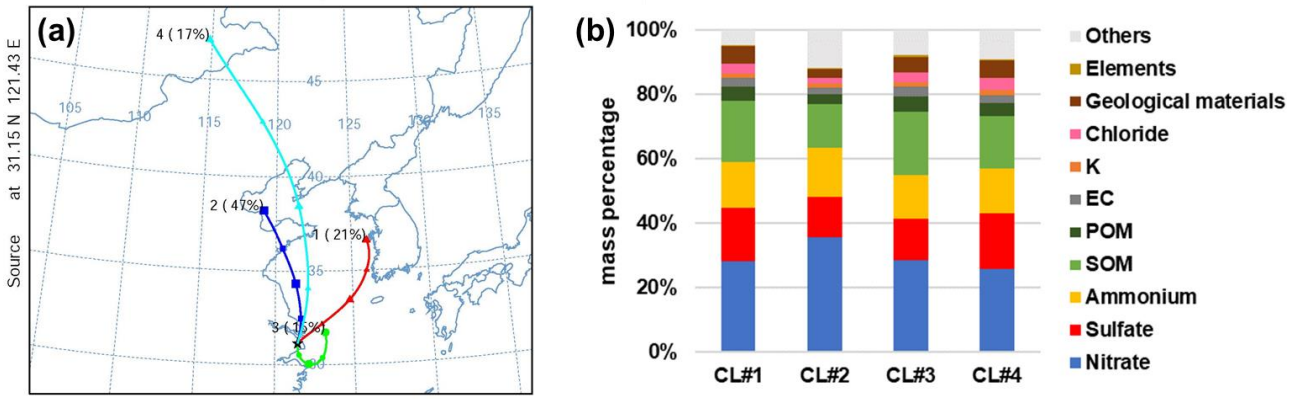

Figure S5. (a) Distribution of the 48-hour backward trajectory clusters arriving at SAES site at 100m above sea level during the campaign; (b) $PM_{2.5}$ chemical compositions under the influences of different clusters

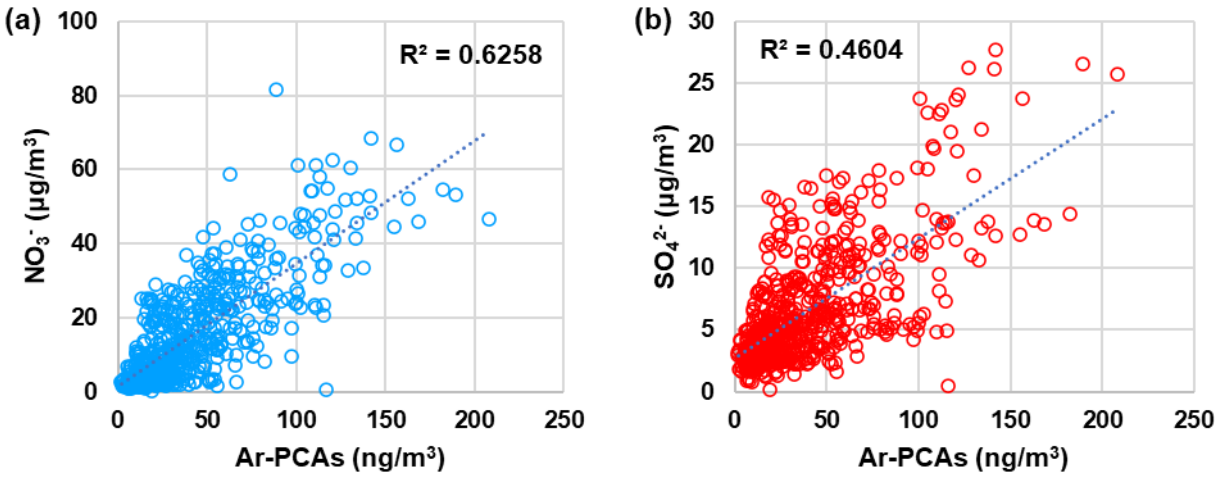

Figure S6. Scatter plots of hourly concentrations of Ar-PCAs versus (a) nitrate and (b) sulfate.

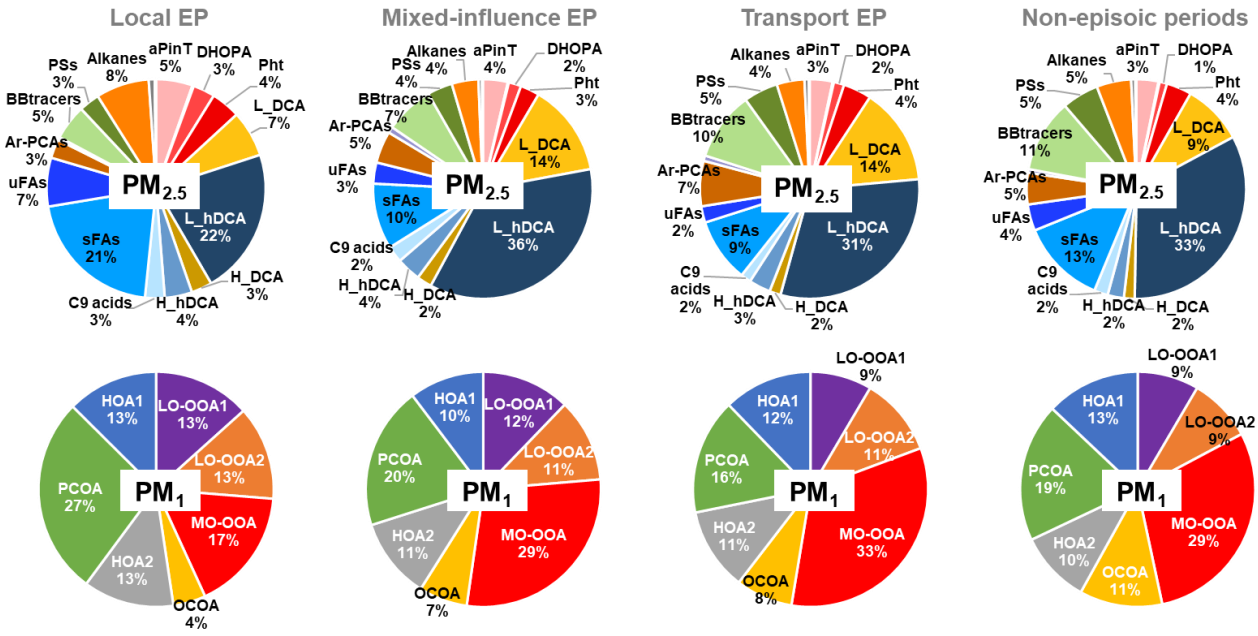

Figure S7. Mass proportions of 18-organic molecular groups in $PM_{2.5}$_OA measured by the TAG system and 7-source factors in PM_1_OA derived from AMS during the local episodes, mixed-influence episodes, transport episodes, and non-episodic periods, respectively.

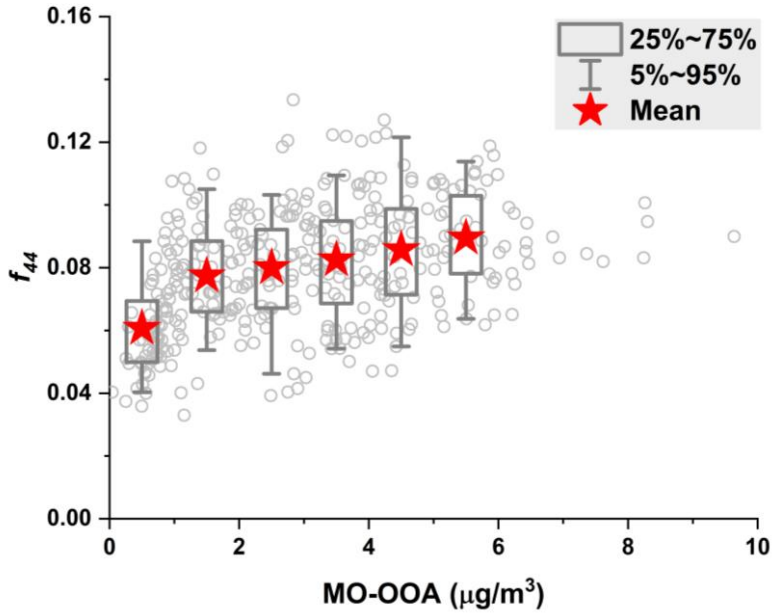

Figure **S8**. f_{44} as a function of MO-OOA concentration bins.

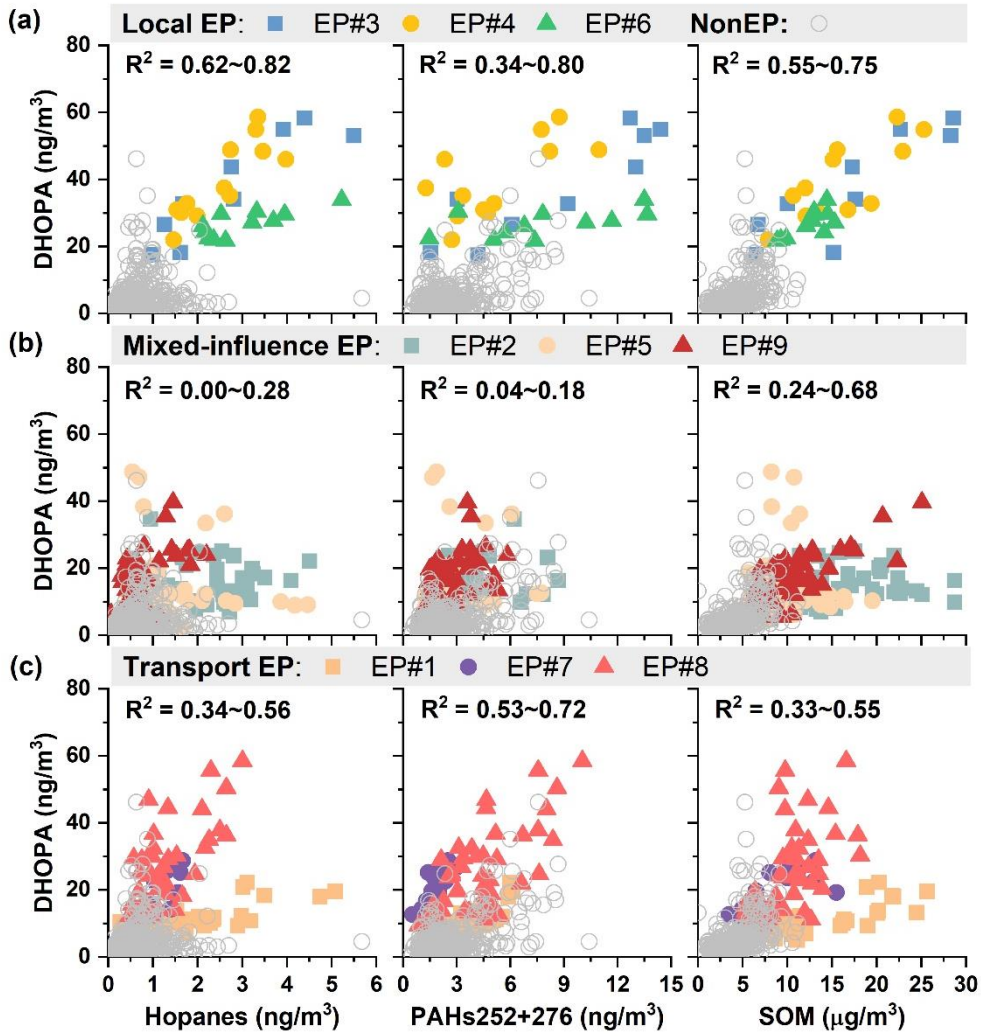

130

Figure S9. Correlations of DHOPA versus hopanes, PAHs and SOM during (a) local, (b) mixed-influence and (c) transport episodes. PAHs252+276 represents the sum of hourly concentrations of BbF, BkF, BaF, BeP, BaP, IcdP, BghiP measured during the campaign.

Text S3. Estimation of aromatic SOA

A modified tracer-based method for estimating aromatic SOA was proposed in Gao et al. (2019) and Zhang et al. (2021a), which has taken into consideration of equilibrium gas-particle partitioning of semi-volatile products. In this method, the hourly concentration of DHOPA, the oxidation product of monoaromatic compounds, is predicted with the following equations:

$$[DHOPA] = \sum_{i=1}^{N} \alpha_i \cdot [VOC_{i,consumed}] \quad (4)$$

$$[VOC_{i,consumed}] = VOC_{i,t} \times (\exp(k_i[OH]\Delta t) - 1) \quad (5)$$

$$[OH]\Delta t = \frac{1}{k_X - k_B} \times (ln\frac{[X]}{[B]}\Big|_{t=t_0} - ln\frac{[X]}{[B]}\Big|_{t=t}) \quad (6)$$

where the mass yield values (α_i) of DHOPA from a specific aromatic precursor *i* were obtained from (Al-Naiema et al., 2020), and k_i is the reaction rate coefficient of precursor *i* with OH radical. Equations (5) and (6) estimate the VOC precursors consumed (Gouw et al., 2018; Borbon et al., 2013; Yuan et al., 2012; Y. Zhu et al., 2017). Due to the predominant presence of toluene and xylenes in urban area (Al-Naiema et al., 2020; Kleindienst et al., 2007; Zhang et al., 2021a), only include these two aromatic precursors were considered in the calculation. In other words, $[VOC_{i,\ consumed}]$ in these equations refers to the consumed mass concentrations of toluene and xylenes by OH radicals, and their corresponding α_i values were 0.0019 for toluene and 0.00090 for xylenes under high-NO_x conditions. Note that our monitoring site had an average NO level at 10.4 ± 19.7 ppb (>1 ppb) and VOCs/NO_x ratio at 1.1 ± 0.7 (<10) during the campaign, consistent with the high NO_x conditions created in the chamber studies. $\frac{[X]}{[B]}\Big|_{t=t}$ is the measured ratio of m+p-xylene to benzene at time t. $\frac{[X]}{[B]}\Big|_{t=t_0}$ represents the concentration ratio in fresh emission before aging begins, which is assumed to be constant during the investigation period. The initial emission ratio was determined by conducting a linear fit on a selected dataset of m+p-xylene and benzene ambient concentrations measured in the early morning (0:00-6:00 A.M.) and with ratios of xylenes to benzene fell in the top 10% range. The ratio is calculated to be 3.5 ppb/ppb, which is close to the slope of the upper "edge" in the scatterplot (Figure S10).

The estimated hourly DHOPA values using equations (4)-(6) are in good agreement with ambient measurements as shown in Figure S11, providing confidence that this modified method reasonably describes the formation and partitioning of DHOPA from multiple aromatic hydrocarbon precursors at this site. Subsequently, semi-volatile mono-aromatic SOA (SemiASOA) and total mono-aromatic SOA (TotalASOA), the latter of which includes more-oxidized aromatic SOA (MoASOA) like oligomers and dicarbonyl compounds, are estimated by the following equations proposed by Zhang et al. (2021a). Then MoASOA can be estimated by subtracting SemiASOA from TotalASOA:

$$SemiASOA = \frac{[DHOPA]}{f_{SOA}} \quad (7)$$

$$TotalASOA = \frac{[DHOPA]}{0.0020} \quad (8)$$

$$MoASOA = TotalASOA - SemiASOA \quad (9)$$

where f_{SOA} is the mass ratio of particle-phase DHOPA to SOA, which can be calculated by equation (10). The mass yield of DHOPA (α) in equation (10) is defined as the ratio of the amount of DHOPA produced to the amount of precursor VOC reacted, and β_i is the mass yield of an individual semi-volatile product *i*. In this study, α and β_i values for toluene and xylene under high NO_x environment were adopted from Zhang et al. (2021a). $F_{p,t}$ and $F_{p,i}$ are the fraction of DHOPA and semi-volatile products in the absorbing OM phase, respectively, which were estimated using equation (11) and (12), respectively. C_{OA} in the equations

represents the mass concentrations of organic aerosols, which were estimated from summing SOM and POM calculated in Section 2.2.2. The K_{OM} in equation (11) is the absorptive gas/particle partitioning coefficient of DHOPA and C_i^* in equation (12) is the saturation mass concentration of the products oxidized from toluene and xylene, both values of which were also adopted from Zhang et al. (2021a).

$$f_{SOA} = \frac{\alpha F_{p,t}}{\sum_{i=1}^{N} \beta_i \cdot F_{p,i}} \tag{10}$$

$$F_{p,t} = \left(1 + \frac{1}{K_{OM} C_{OA}}\right)^{-1} \tag{11}$$

$$F_{p,i} = \left(1 + \frac{C_i^*}{C_{OA}}\right)^{-1} \tag{12}$$

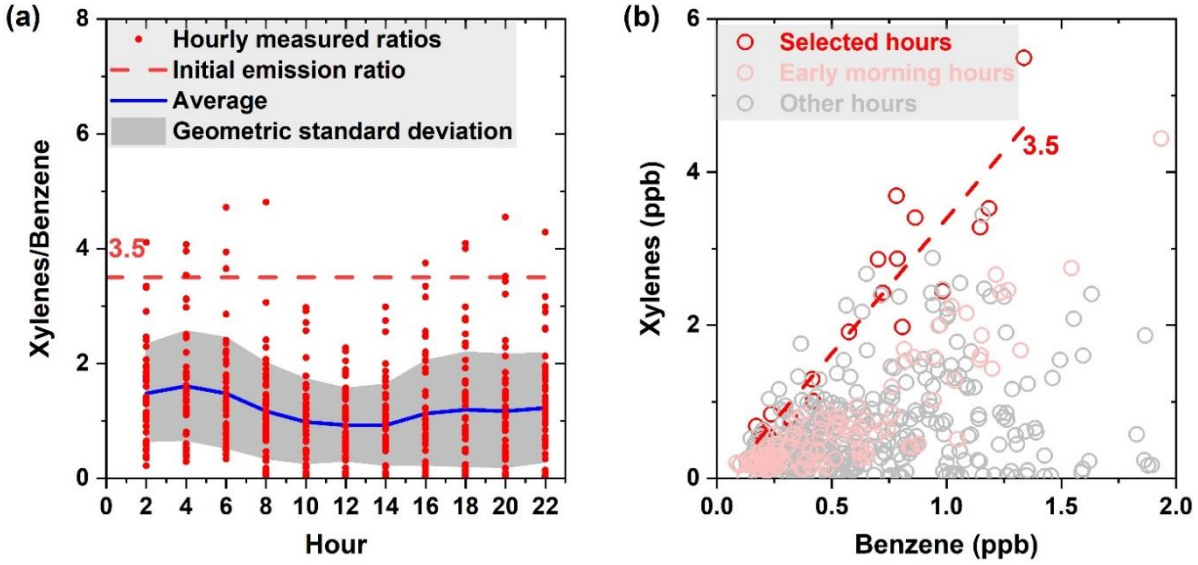

Figure S10. (a) Diurnal variations of m+p-xylene/benzene concentration ratios during the campaign. Red dots are measured hourly ratios. Blue line indicates hourly geometric average, and gray area represents geometric standard deviations; (b) scatter correlation of m+p-xylene with benzene. Data selected for estimation of initial emission ratio were colored with red. The dashed red line in both graphs show the estimated initial emission ratio of m+p-xylene/benzene which is 3.5.

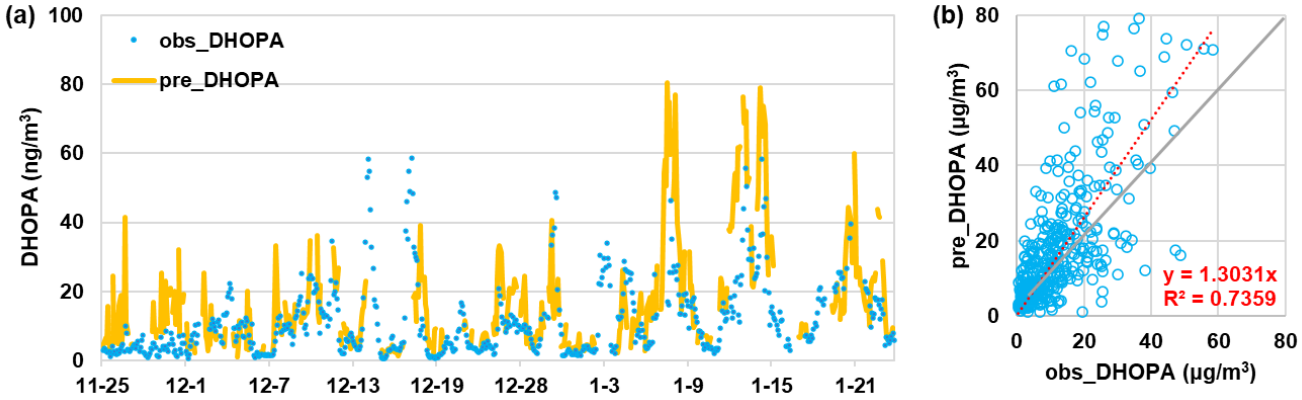

Figure S11. (a) Predicted and observed hourly concentrations of DHOPA during the campaign; (b) scatter plots of predicted and observed hourly DHOPA. Dashed red line is the linear fit line with slope forced to zero based on all hourly dataset and solid grey line is the 1:1 line.

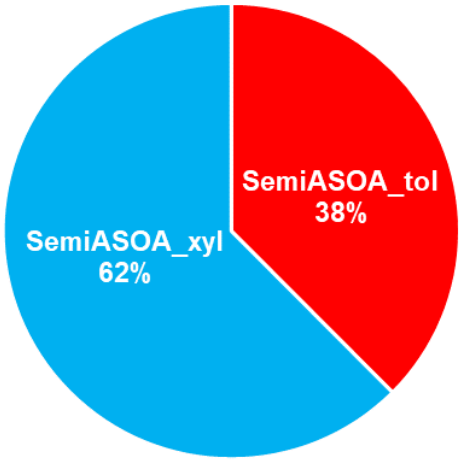

Figure S12. Predicted contributions to DHOPA from toluene and xylene pathways under high-NO_x conditions.

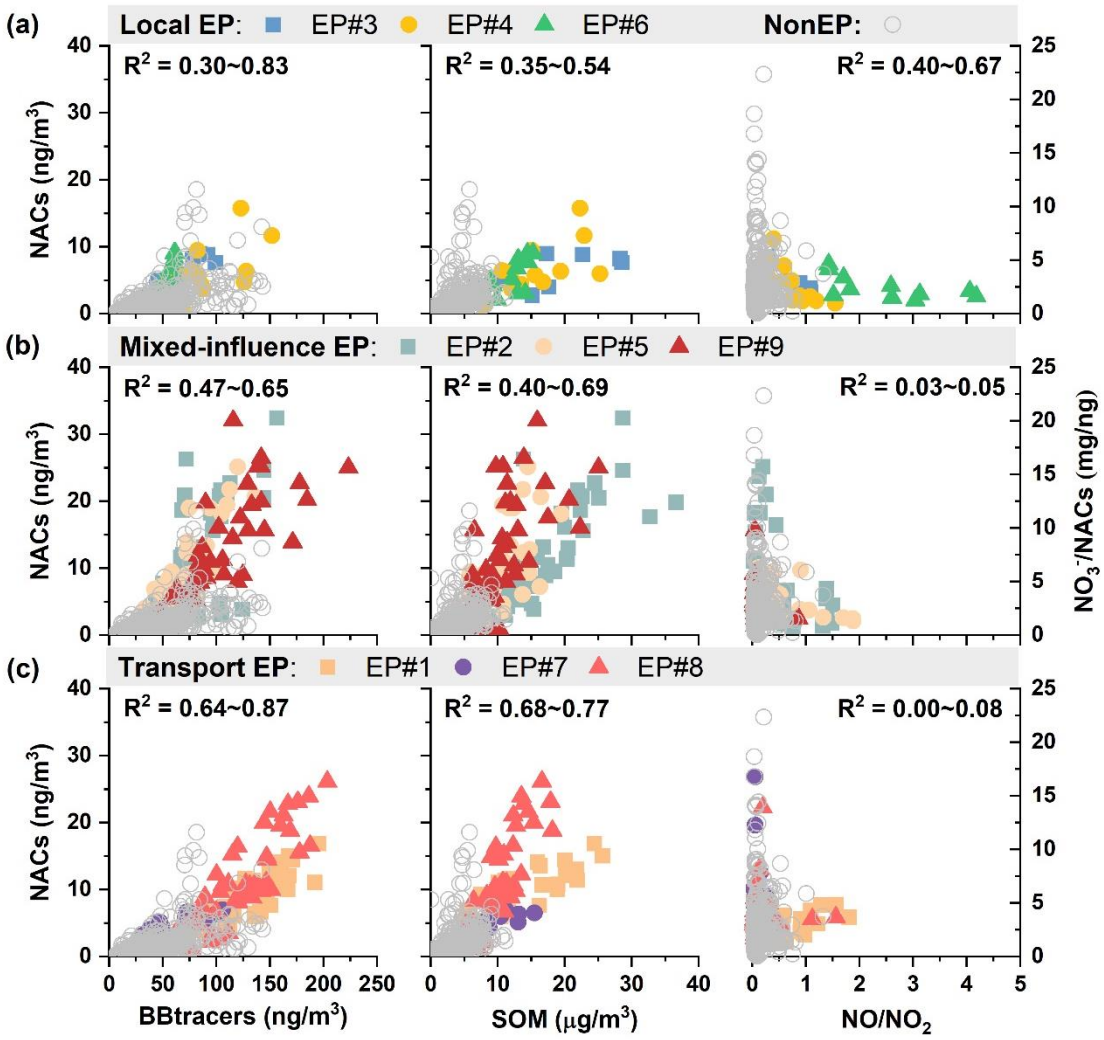

Figure S13. Correlations of NACs versus biomass burning tracers (BBtracers), SOM and nitrate to NACs ratios versus NO/NO_2 ratios during (a) local, (b) mixed-influence and (c) transport episodes.

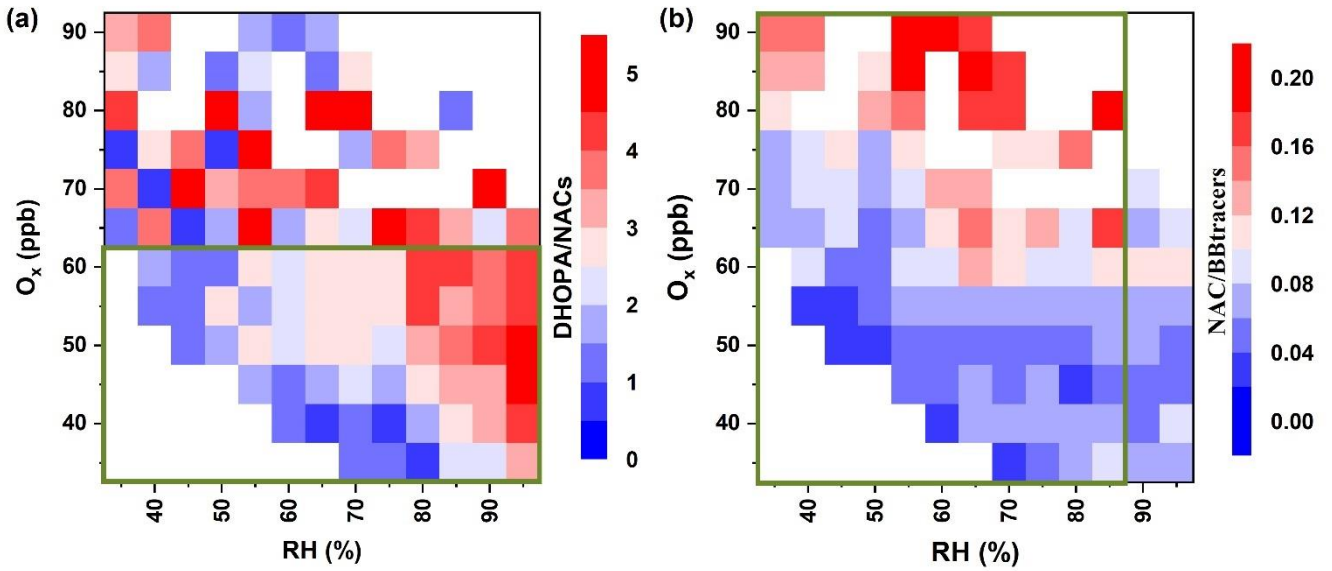

Figure S14. RH versus O_x dependence of the mass ratios of (a) DHOPA to NACs and (b) NACs to biomass burning tracers during the field campaign.

References

Al-Naiema, I., Offenberg, J. H., Madler, C. J., Lewandowski, M., Kettler, J., Fang, T. and Stone, E. A.: Secondary organic aerosols from aromatic hydrocarbons and their contribution to fine particulate matter in Atlanta, Georgia, Atmospheric environment (1994), 223, 117227, 10.1016/j.atmosenv.2019.117227, 2020.

Borbon, A., Gilman, J. B., Kuster, W. C., Grand, N., Chevaillier, S., Colomb, A., Dolgorouky, C., Gros, V., Lopez, M., Sarda-Esteve, R., Holloway, J., Stutz, J., Petetin, H., McKeen, S., Beekmann, M., Warneke, C., Parrish, D. D. and de Gouw, J.,A.: Emission ratios of anthropogenic volatile organic compounds in northern mid-latitude megacities: Observations versus emission inventories in Los Angeles and Paris, Journal of geophysical research. Atmospheres, 118, 2041-2057, 10.1002/jgrd.50059, 2013.

Bressi, M., Sciare, J., Ghersi, V., Mihalopoulos, N., Petit, J. -., Nicolas, J. B., Moukhtar, S., Rosso, A., Féron, A., Bonnaire, N., Poulakis, E. and Theodosi, C.: Sources and geographical origins of fine aerosols in Paris (France), Atmospheric chemistry and physics, 14, 8813-8839, 10.5194/acp-14-8813-2014, 2014.

Gouw, J. A., Gilman, J. B., Kim, S. -, Alvarez, S. L., Dusanter, S., Graus, M., Griffith, S. M., Isaacman-VanWertz, G., Kuster, W. C., Lefer, B. L., Lerner, B. M., McDonald, B. C., Rappenglück, B., Roberts, J. M., Stevens, P. S., Stutz, J., Thalman, R., Veres, P. R., Volkamer, R., Warneke, C., Washenfelder, R. A. and Young, C. J.: Chemistry of Volatile Organic Compounds in the Los Angeles Basin: Formation of Oxygenated Compounds and Determination of Emission Ratios, Journal of geophysical research. Atmospheres, 123, 2298-2319, 10.1002/2017JD027976, 2018.

Gao, Y., Wang, H., Zhang, X., Jing, S., Peng, Y., Qiao, L., Zhou, M., Huang, D. D., Wang, Q., Li, X., Li, L., Feng, J., Ma, Y. and Li, Y.: Estimating Secondary Organic Aerosol Production from Toluene Photochemistry in a Megacity of China, Environ. Sci. Technol., 53, 8664-8671, 10.1021/acs.est.9b00651, 2019.

Huang, D. D., Zhu, S., An, J., Wang, Q., Qiao, L., Zhou, M., He, X., Ma, Y., Sun, Y., Huang, C., Yu, J. Z. and Zhang, Q.: Comparative Assessment of Cooking Emission Contributions to Urban Organic Aerosol Using Online Molecular Tracers and

Aerosol Mass Spectrometry Measurements, Environ. Sci. Technol., 55, 14526–14535, 10.1021/acs.est.1c03280, 2021.

Kleindienst, T. E., Jaoui, M., Lewandowski, M., Offenberg, J. H., Lewis, C. W., Bhave, P. V. and Edney, E. O.: Estimates of the contributions of biogenic and anthropogenic hydrocarbons to secondary organic aerosol at a southeastern US location, Atmospheric environment (1994), 41, 8288-8300, 10.1016/j.atmosenv.2007.06.045, 2007.

Waked, A., Favez, O., Alleman L, Y., Piot, C., Petit, J., Delaunay, T., Verlinden, E., GOLLY, B., Besombes, J. and Jaffrezo, J.: Source apportionment of PM_{10} in a north-western Europe regional urban background site (Lens, France) using positive matrix factorization and including primary biogenic emissions, Atmospheric chemistry and physics, 14, 3325-3346, 10.5194/acp-14-3325-2014, 2014.

Yuan, B., Shao, M., de Gouw, J., Parrish, D. D., Lu, S., Wang, M., Zeng, L., Zhang, Q., Song, Y., Zhang, J. and Hu, M.: Volatile organic compounds (VOCs) in urban air: How chemistry affects the interpretation of positive matrix factorization (PMF) analysis, Journal of Geophysical Research: Atmospheres, 117, n/a, 10.1029/2012JD018236, 2012.

Zhang, J., He, X., Gao, Y., Zhu, S., Jing, S., Wang, H., Yu, J. Z. and Ying, Q.: Assessing Regional Model Predictions of Wintertime SOA from Aromatic Compounds and Monoterpenes with Precursor-specific Tracers, Aerosol and air quality research, 21, 210233, 10.4209/aaqr.210233, 2021a.

Zhu, Y., Yang, L., Kawamura, K., Chen, J., Ono, K., Wang, X., Xue, L. and Wang, W.: Contributions and source identification of biogenic and anthropogenic hydrocarbons to secondary organic aerosols at Mt. Tai in 2014, Environ. Pollut., 220, 863-872, 10.1016/j.envpol.2016.10.070, 2017.